Journal of Environmental Management 213 (2018) 549–554

Contents lists available at ScienceDirect

Journal of Environmental Management

journal homepage: www.elsevier.com/locate/jenvman

Research article

Lanthanum-doped silica xerogels for the removal of fluorides from waters

M. Hernández-Campos [a, b], A.M.S. Polo [a], M. Sánchez-Polo [a, *], J. Rivera-Utrilla [a], M.S. Berber-Mendoza [b], G. Andrade-Espinosa [c], M.V. López-Ramón [d]

[a] Department of Inorganic Chemistry, University of Granada, 18071, Granada, Spain
[b] Center of Postgraduate Research and Studies, Faculty of Engineering, University Autonomous of San Luis Potosí, Av. Dr. M. Nava No. 8, San Luis Potosí, SLP, 78290, Mexico
[c] Valle de Morelia Technological Institute, Km. 6.5 Carretera Morelia-Salamanca, Los Angeles, 58100, Morelia, Mich., Mexico
[d] Department of Inorganic and Organic Chemistry, University of Jaén, 23071, Jaén, Spain

ARTICLE INFO

Article history:
Received 24 October 2017
Received in revised form
31 December 2017
Accepted 3 February 2018
Available online 19 February 2018

Keywords:
Silica xerogels
Dopant
Lanthanum
Fluoride removal

ABSTRACT

The objective of this study was to determine the influence of different operational variables on fluoride (F^-) removal from waters using lanthanum (La)-doped silica xerogels and the mechanisms involved in this process. Accordingly, four xerogels were synthesized, one acting as blank (X-B), two doped with $LaCl_3$ and dried at different temperatures (X-LaCl and X-LaCl-M), and a fourth doped with La_2O_3 (X-LaO). The results show that fluorides are only removed when La-doped xerogels are utilized. In addition, X-LaCl yielded the highest adsorption capacity, removing 28.44% of the initial fluoride concentration at a solution pH of 7. Chemical characterization of materials confirmed that fluoride removal from waters is due to the precipitation of LaF_3 on the surface of La-doped xerogels. The presence of dissolved organic matter on the aqueous solution also reduce the removal capacity of La xerogels. Finally, analysis of the influence of solution pH revealed that the adsorption capacity of all xerogels was highest at a solution pH of 7.

© 2018 Elsevier Ltd. All rights reserved.

1. Introduction

Fluoride (F^-) contamination of waters that supply some populations is an endemic problem worldwide (Amini et al., 2008) due to the dissolution of minerals such as fluorite [CaF_2], apatite [$Ca_5(PO_4)_3(F, Cl, OH)$], and cryolite [Na_3AlF_6] when they come in contact with groundwaters (Edmunds and Smedley, 2013). Human health can be affected by the insufficient or excessive presence of fluoride. Thus, dental caries can develop at concentrations between 0 and 0.5 m/L, while dental fluorosis can appear at concentrations between 1.5 and 4 mg/L, and there is an increased risk of skeletal fluorosis, paralysis, disability, or even death at higher fluoride concentrations (Fawell and Bailey, 2006). The most frequent treatments for fluoride removal from waters are membrane separation (Richards et al., 2010), ion exchange resins, electrodialysis (Mohapatra et al., 2009), and adsorption (Landín-Rodríguez, 2006; Leyva-Ramos et al., 2008; Metcalf et al., 2003; Teutli-Sequeira et al., 2013; Yakun et al., 2011). Adsorption is the most practical and low-cost method for fluoride removal, requiring material that is mechanically resistant and selective with high fluoride removal capacity.

As a member of the halide group, the behavior of fluoride should be the same as that of chloride, iodide, or bromide. Studies have been conducted on its removal from natural waters by adsorption using silver-doped carbon aerogels. Sánchez-Polo et al. (2007a,b) investigated bromide and iodide removal from drinking water silver-doped carbon aerogels, and silver-doped activated aerogels, finding an increased adsorption capacity, especially in the aerogels samples activated by heating at 1173 K in CO_2 flow (100 cm^3/min) for 1 h. It is interesting to note that bromide and iodide adsorption on columns filled with silver-doped aerogels was very efficient. The results obtained show a high column volume breaking point but low height of the mass transfer zone, regardless of the halide used.

Fluoride removal from waters has been studied using activated alumina (Cheng et al., 2014; Craig et al., 2017), bone char (Craig et al., 2017), zeolite modified with Al^{+3} and La^{+3} (Teutli-Sequeira et al., 2013), and spheres of alginate doped with La(III) (Yakun

* Corresponding author.
E-mail address: mansanch@ugr.es (M. Sánchez-Polo).

https://doi.org/10.1016/j.jenvman.2018.02.016
0301-4797/© 2018 Elsevier Ltd. All rights reserved.

et al., 2011). Silica xerogels (SXGs) are currently the most widely studied group of aerogels and are (Teutli-Sequeira et al., 2013) of major interest in the field of wastewater treatment (Han et al., 2016; Mohammadi and Moghaddas, 2015; Perdigoto et al., 2012). SXGs have a large surface area due mainly to the presence of mesopores. They exhibit a greater adsorption capacity in comparison to other frequently used adsorbents, with high mechanical resistance. They proved to be good adsorbent materials when their surface is modified with nanoparticles of iron or other metals that form oxides or hydroxides (Andrade-Espinosa et al., 2010; Andrade Espinosa, 2011; Martınez and Ruiz, 2002). However, no research has been published on SXGs activated with lanthanum (La). With this background, the objectives of this study were to: i) synthesize La(III)-doped SXGs for effective fluoride removal from waters, ii) characterize their physicochemical (X-Ray diffraction (XRD), X-ray photoelectron spectroscopy (XPS), Zeta potential and isoelectric point (IEP), and Fourier transform infrared spectroscopy (FTIR)), textural and morphological (N_2 physisorption at 77 K, and high-resolution scanning electron microscopy (HSEM)) properties, and iii) evaluate the influence of operating variables (pH and organic matter) on fluoride adsorption efficiency.

2. Materials and reagents

The following analytical grade reagents were used for the SXG synthesis and evaluation of fluoride removal. Tetraethoxysilane (TEOS, 99.99%), isopropanol (IPrOH, 99.9%), heptahydrate La chloride ($LaCl_3$ x $7H_2O$), La oxide (La_2O_3, 99.95%), hydrochloric acid (HCl, 36.5–38%), ammonium hydroxide (NH_4OH, 28.9%), nitric acid (HNO_3, 69%), sodium fluoride (NaF), sodium hydroxide (NaOH), sodium nitrate ($NaNO_3$), TISAB. All the solutions were prepared using ultrapure water.

3. Experimental

3.1. Xerogel synthesis by two-step sol-gel process

The precursor used was tetraethoxysilane, which was dissolved in deionized water in the presence of isopropanol and hydrochloric acid as acid catalyst to favor hydrolysis, maintaining the solution at a constant temperature of 60 °C for 1 h. The molar ratio used in the synthesis was TEOS: IPrOH: $H_2O = 1:4:10$ (Andrade Espinosa, 2011), given that high molar ratios of H_2O with TEOS favor complete hydrolysis, facilitating polymer chain cross-linking and producing a tridimensional interconnected siloxane network (Martınez and Ruiz, 2002). Hydrochloric acid (1 M) was gradually added until pH = 2 was reached during synthesis in the sol step, followed by a condensation reaction through the addition of ammonium hydroxide (0.6 M) as basic catalyst, reaching pH = 6. The structure consolidated and xerogel ageing began after gelation for 4–6 h at 60 °C. After obtaining the SXG matrix, it was impregnated with La(III) for 3 days, using a solution of 0.1 M $LaCl_3 \cdot 7H_2O$, and it was then washed with IPrOH for 2 days and maintained at a constant temperature of 60 °C for 3 days. Another SXG was also synthesized and impregnated with pure La_2O_3 before its condensation. Four xerogels were prepared following the next procedure. Two doped with La^{+3}, based on $LaCl_3 \cdot 7H_2O$ (one dried at 60 °C [X-LaCl] and the other heated at 450 °C after drying at 60 °C [X-LaCl-M]), a third doped with La_2O_3 (X-LaO), and a reference blank (X-B). They were characterized by N_2 adsorption at 77 K, HSEM, Zeta potential measurement, FTIR, XRD, and XPS (see details below).

3.2. Xerogel characterization

Xerogel surface area and pore size and volume were determined using N_2-physisorption equipment at 77 K (Micromeritics ASAP 2010 V4.02). Zeta potential was determined by adding a specific mass of SXG to different volumetric ratios of HNO_3, $NaNO_3$, and NaOH at a concentration of 0.01 M for 7 days at constant temperature under agitation. Potential values were determined in a nano-ZS ZETASIZER. Morphological characteristics were evaluated by HSEM using a scanning electron microscope (Hitachi S-510). Samples were covered with a thin layer of gold to provide conductive properties for elemental surface microanalysis. The SXGs were analyzed in the mid-infrared region, from 670 to 4000 cm^{-1}, using the attenuated total reflectance (ATR) technique. The SXGs were analyzed by XRD using a BRUKER D8 VENTURE diffractometer and BRUKER LYNXEYE detector with Cu Kα radiation (λ) = 1.5406 Å, voltage of 40 KV, current of 40 mA, in the range of 2θ = 5° - 80°, step size ≈ 0.02°, and 96 s/step. SXG surface chemistry was analyzed using a Kratos Axis Ultra-DLD X-ray photoelectron spectrometer.

3.3. Fluoride ion adsorption

Adsorption isotherms were obtained to study the adsorption process and evaluate the capacity of the SXGs to remove fluoride ions from the medium. Adsorption was analyzed by evaluating the effects of: i) pH (range 5–9), ii) presence of organic matter (5, 50, and 250 mg/L) and v) use of groundwater intended for human consumption. Fluoride concentration was measured by using a selective electrode (Crison).

4. Results and discussion

4.1. Silica xerogel characterization

Fig. 1 depicts the nitrogen adsorption isotherms for the SXGs under study. According to the classification of Sing, the X-B xerogel can be classified as type I, characteristic of microporous solids, in which a plateau is reached after micropore filling, whereas the three La-doped xerogels are type IV, characteristic of mesoporous materials. The initial part of a type IV isotherm corresponds to monolayer filling, while the inflection point of the curve, after which multilayer adsorption begins, is associated with the relative nitrogen pressure produced by monolayer filling. Fig. 1 B, C, and D depict the isotherms of the three La-doped xerogels, showing a hysteresis cycle corresponding to capillary condensation in mesopores.

Table 1 exhibits the results of applying the BET equation to the N_2 isotherms, showing that the surface area was smaller in the non-La-doped (X-B) *versus* La-doped samples. The surface area of sample X-B was 506.94 m^2/g, the pore volume 0.25 cm^3/g, and the mean pore diameter 19.66 cm^3/g, identifying it as a microporous material according to the IUPAC classification. In comparison to this sample, the surface area, pore volume, and mean pore diameter were higher in samples X-LaCl and X-LaCl-M, which may result from their doping with lanthanum chloride, which increases the surface area through the adherence of its nanoparticles. Sample X-LaO had the largest surface area (732.81 m^2/g), pore volume (0.81 cm^3), and mean pore diameter (44.38 Å), which may be attributable to spaces created by the entry of La oxide particles into the xerogel structure, given the simultaneous gelation and impregnation of this material. The mechanism of La^{+3} integration into the xerogel starts with the adsorption of La^{3+} ions and silanol (SiOH) groups, which continue to be present in the xerogel. Two unpaired electrons of the oxygen atom in the silanol group are shared with La(III), and a water molecule rapidly interacts with the hydroxyl by the nucleophilic attack of two unpaired electrons that promote H^+ as a good salient group that pass to the solution; the water molecules present in the solution interact with La, forming

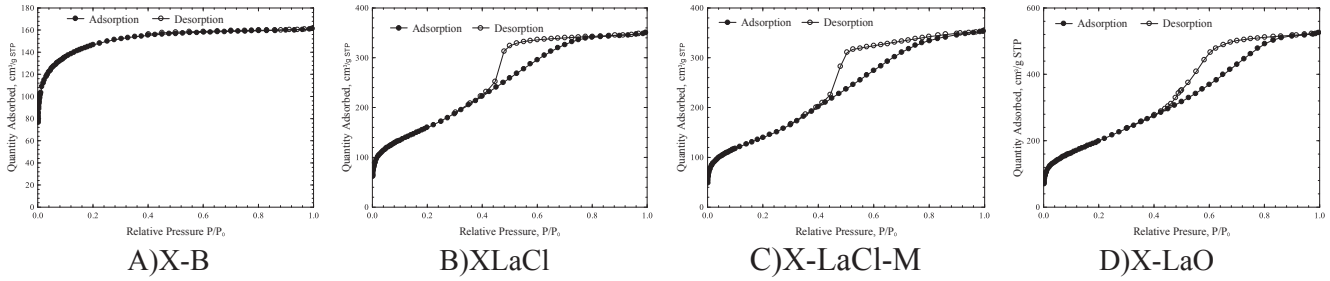

Fig. 1. N_2 adsorption isotherms of the SXG.

Table 1
Textural properties of the SXGs.

Material	Surface Area (m^2/g)	Pore Volume (cm^3/g)	Pore Size (Å)
X-B	506.94	0.25	19.66
X-LaCl	579.67	0.54	37.36
X-LaCl-M	509.01	0.55	42.97
X-LaO	732.81	0.81	44.38

the La hydroxo complex ($La\,OH_2^+$) and immobilizing La^{3+} in the Si matrix. The La^{3+} bound to the Si matrix can subsequently undergo nucleophilic attack by two unpaired electrons from the oxygen of the hydroxyl group of the dissolved isopropanol. Another isopropanol molecule carries out the same nucleophilic attack with the hydroxyl group proton that binds with the La ion, transforming it into a salient group and leaving the oxygen with an electron deficiency that is rapidly covered by OH^- present in the solution, giving rise to the formation of LaOOH. The surface area of SXGs has been reported to range between 580 and 890 m^2/g when NH_4OH or $I\text{-}Pr_{OH}$ are used as basic catalyst and between 685 and 1046 m^2/g when TEOS is used as precursor and HCl as catalyst, with a volume between 0.41 and 2.31 cm^3/g [20]. All SXGs reported in the literature have been mesoporous, with pore sizes ranging between 23.9 and 97 Å. In the present study, xerogel X-B was microporous, with a pore size of 19.6 Å, while the La-doped SXGs were mesoporous, with pore sizes ranging between 37.36 and 44.38 Å. These characterizations are consistent with the information deduced from N_2 adsorption isotherms (Fig. 1).

Adsorbent-adsorbate electrostatic interactions are determined by the adsorbent surface charge and its variation with solution pH. The behavior of zeta potential values as a function of medium pH for each xerogel and also reports their IEP values, indicating the acid character of all samples, with a value of 2.6 for X-B and 3.35 for the La-doped xerogels. Fig. 2 depicts the infrared spectra of the xerogels, revealing the presence of the following functional groups: symmetric Si-O-Si, at wavelength of 800 cm^{-1}; Si-OH groups at 940 cm^{-1}, and asymmetric Si-O-Si, which is at 1045 cm^{-1} and shows the highest transmittance in all SXGs. As evidenced in the behaviors of the X-B, X-LaCl, and X-LaO xerogels were similar, with a constant base matrix whether doped or not, whereas X-LaCl-M, which was dried at higher temperature, showed a different vibration of the bond and its reduced transmittance and wavelength in Si-OH functional groups. The presence of these functional groups in Si gels is attributable to hydrolysis and polycondensation reactions during their synthesis (Reactions 1–3). Fig. 3 depicts the XRD diagrams of the SXGs, revealing their completely amorphous Si structure in 2 $\theta = 25°$, with poorly defined diffraction peak (Jung et al., 2012; Lowell et al., 2012). This agrees with the FTIR findings of a predominance of the amorphous Si-O-Si functional group over the symmetrical Si-O-Si group. Fig. 4 depicts the general XPS spectrum of the four SXGs, showing the presence of Si-O-H and Si-O bonds with signals corresponding to O at 532 eV and Si at 102 eV (Ivanova et al., 1996).

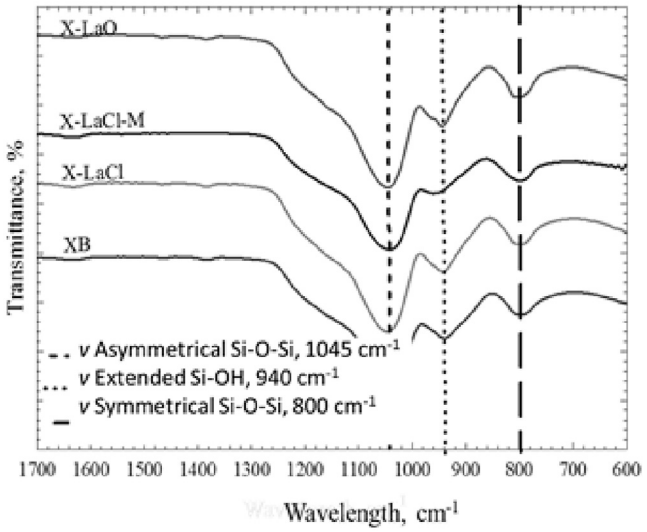

Fig. 2. FTIR of the SXGs obtain.

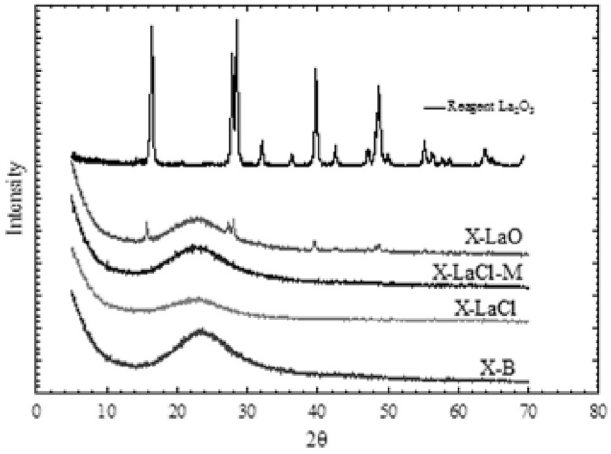

Fig. 3. X-ray diffractogram of the SXGs and La_2O_3 reagent.

$$\text{Hydrolysis: } Si(OR)_4 + 4H_2O \rightarrow Si(OH)_4 + 4ROH \quad (1)$$

$$\text{Polycondensation: } Si(OH)_4 + Si(OH)_4 \rightarrow 2SiO_2 + 4H_2O \quad (2)$$

$$Si(OR)_4 + Si(OH)_4 \rightarrow 2SiO_2 + 4ROH \quad (3)$$

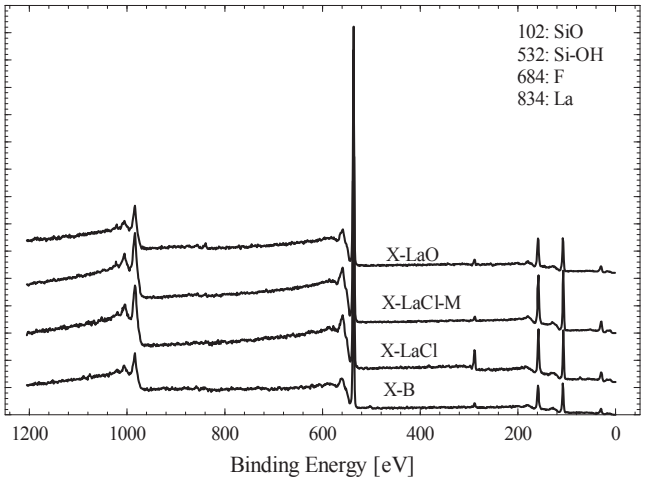

Fig. 4. XPS spectra of the four SXGs before F^- adsorption.

4.2. Fluoride adsorption process

Fig. 5 depicts microphotographs of the SXGs after their contact with fluoride. X-B (Fig. 5A) shows no appreciable surface change; X-LaCl (Fig. 5B) evidences fluoride deposits from its precipitation as La_3F, which remains on the surface because the Kps value is 4×10^{-17}.

The same behavior is observed on the SXGs of X-LaCl-M and X-LaO with adsorbed fluoride, as shown in Fig 5C and D, respectively; thus, when F^- forms LaF_3 it does not crystallize on the surface and only remains on the surface of SXGs that preserve their amorphous structure. The peaks present in the X-LaO diffractogram correspond to the crystalline compound of La_2O_3, as demonstrated in the diffractogram of pure La_2O_3. Fig. 6 depicts the XR diffractograms of the SXGs after F^- adsorption, showing that the peak in $2\theta = 25°$ is better defined, increasing its crystallinity on the surface of the material. The composition of X-LaO is modified by contact with fluoride, with the disappearance of La_2O_3 peaks. The SXGs were analyzed by XPS after contact with fluoride. The general spectra of the SXGs depicted in Fig. 7 show that the binding energies of Si and O did not change in X-B, X-LaCl-M, or X-LaO samples; however, the intensity of the Si peak (102 eV) decreased in X-LaCl, in which the signal corresponding to La appeared in 3d5/2 at 834 eV and that for F^- was at 684 eV. These findings confirm the HSEM results in Fig. 5B, showing that X-LaCl has deposits and precipitates that contain La and F (by EDX).

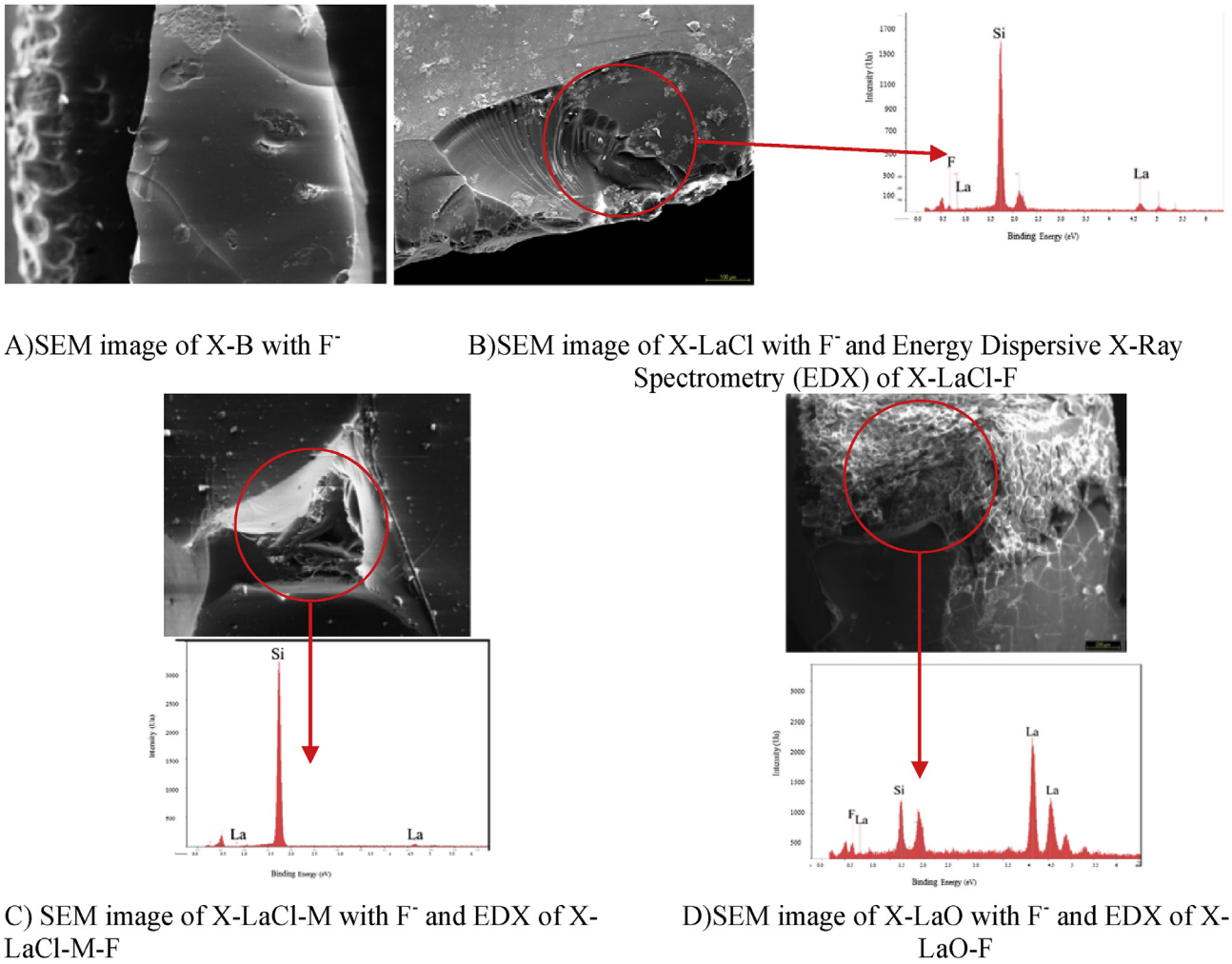

Fig. 5. Microphotographs by HSEM and Energy Dispersive X-Ray Spectrometry (EDX) of SXGs after fluoride adsorption.

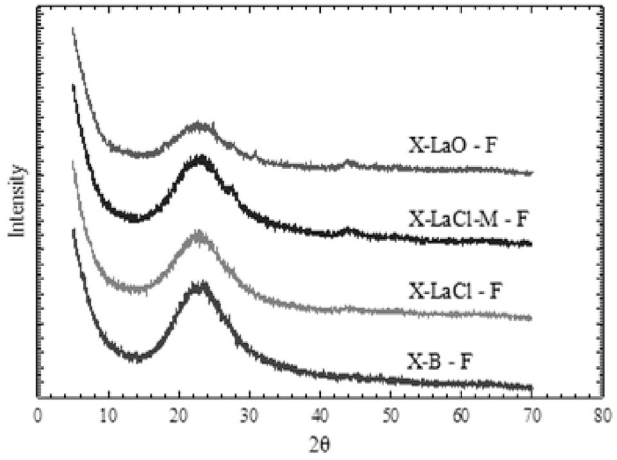

Fig. 6. XR diffractograms of the SXGs after F^- adsorption.

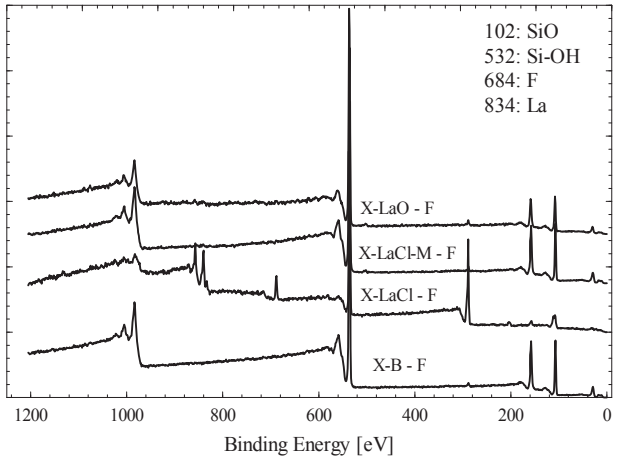

Fig. 7. XPS spectra of the SXGs after fluoride adsorption.

4.2.1. Effect of solution pH

Fig. 8 depicts the effect of pH on the modified SXGs. Fig. 8a shows a reduction in adsorption by X-LaCl xerogel of F^- (baseline concentration of 0.51 mmoles) at higher pH values, from 32.01% at pH = 5 to 19.78% at pH = 9, whereas pH variation had a lesser effect on X-LaCl-M (from 15.06 to 13.01%) and had no substantive impact on adsorption by X-LaO. In general, the adsorption capacity of the material decreases at higher pH because the material is negatively charged above the IEP, and fluoride anions are therefore repelled on its surface. The species diagram of La(III) as a function of pH shows that La hydrolysis is significant in acid conditions and that the dominant species is La(III) (Mohammadi and Moghaddas, 2015) at around pH = 10.5, with $k = 10^{-22,8}$. In addition, fluoride forms weakly ionizable species at acid pH values (<4).

Table 2
F^- mass adsorbed (mmol/g) in the presence of OM.

Material	Adsorption capacity mmol/g			
	Distilled water	[OM] 5 mg/L	[OM] 50 mg/L	[OM] 250 mg/L
XB	2.71	5.18	4.77	–
XLaCl	43.54	46.40	48.89	56.44
XLaCl-M	41.84	48.45	4.12	61.21
XLaO	3.96	6.13	6.88	53.80

4.2.2. Influence of the presence of organic matter (OM)

F^- contamination of water frequently derives from direct contact with the rocks of the subsoil; therefore, OM may also be present. The most widely used method to remove OM is the direct addition of sodium hypochlorite to the water under treatment, but this leaves chlorides in the water that may interfere with fluoride removal. For this reason, the best approach is to eliminate the fluoride before removing the OM. Accordingly, we evaluated F^- removal in the presence of OM by placing a fluoride solution at a concentration of 70 mmol L^{-1} in contact with OM concentrations of 5.50 and 250 mg/L, using fluoride adsorption on the SXGs in distilled water as reference. In a previous experiment, it was observed that OM is not adsorbed on these SXGs. Table 2 lists the F^- mass adsorbed on the four xerogels in the presence of OM, showing that their adsorption capacity generally increased with the presence of OM. In all samples, F^- adsorption was slightly increased by the addition of 5 or 50 mmol/g OM, while a considerably higher increase was obtained when 250 mmol/g OM was added. Given the above results, the increased F^- adsorption on our xerogels in the presence of OM (Table 2) is a highly unexpected finding for which we have no definitive explanation, although it may be related to the increased hydrophobicity of the xerogel surface due to the presence of supramolecular OM conformations. Further studies are warranted in this line to elucidate this interesting behavior of major interest for natural water treatments, because it would permit the removal of large amounts of F^- in the presence of OM. Therefore, according to the present results, SXG can be used for the treatment of well waters with a high NOM load, first adsorbing fluoride and then treating the OM load with sodium hypochlorite.

4.2.3. Influence of water matrix

The composition of tap water varies widely according to its

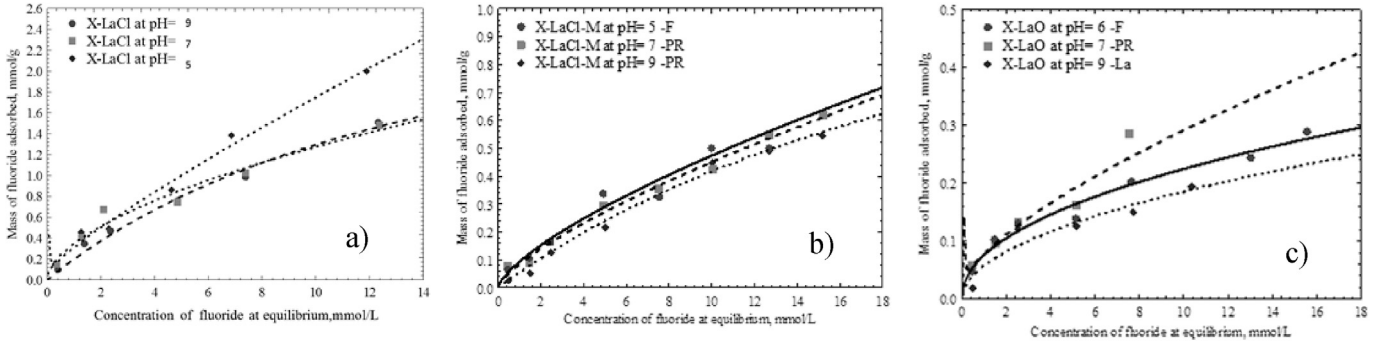

Fig. 8. Adsorption capacity of the SXGs as a function of pH: a) X-LaCl, b) X-LaCl-M, and c) X-LaO.

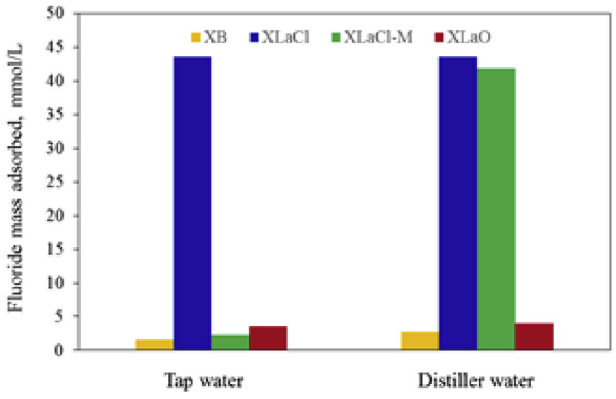

Fig. 9. F^- mass adsorbed on xerogels in distilled water and tap water. $[F^-]_0 = 70$ mmol L^{-1}.

source, with differences in pH, color, hardness, and conductivity. Fluoride adsorption was therefore evaluated using distilled deionized water and tap water. Fig. 9 depicts the amount of F^- mass adsorbed on the SXG samples. This figure shows that the F^- mass adsorbed on X-B and X-LaCl-M was lesser in tap water than in distilled water, with a particularly drastic reduction in adsorption on X-LaCl-M. The F^- mass adsorbed on X-LaCl and X-LaO was similar between distilled and tap water. Hence, X-B and X-LaCl-M are not F^--selective in the presence of other dissolved ions, such as chlorides, nitrates, carbonates, or sulfates, which may compete for surface sites. However, X-LaCl and X-LaO are F^--selective in tap water, indicating the absence of competition with ions in this medium. As noted above, anions (e.g., chlorides, nitrates, or sulfates) may compete for positively charged adsorbent sites in tap water, who used bone char as iron nanoparticle support for arsenic (V) and F^- removal and by Tang et al. (2009) in their study on the behavior of granular iron hydroxides in F^- removal.

A finding of great interest is that the high F^- adsorption capacity of the X-LaCl xerogel is substantially increased in the presence of NOM and is not impaired by the presence of other anions in the medium.

5. Conclusions

These doped SXGs are mesoporous according to nitrogen physisorption analysis. Elemental microanalysis (EDX) of fluoride-treated samples shows that X-LaCl-F and X-LaO-F xerogels present Si, La, and F on deposits, while XPS studies reveal the same elements, with only X-LaCl-F showing the F that confirms the presence of LaF_3. The Zeta potential of the SXGs is negative, with an IEP between 2.6 and 3.35 pH; however, all SXGs demonstrate F^- adsorption capacity despite the electrostatic repulsions produced by their negative charge. Therefore, adsorption may take place by other mechanisms, such as chemisorption. The effect of pH on adsorption capacity differed between X-LaCl and X-LaO xereogels, which achieved maximum capacity at distinct pH values, whereas pH variations had no effect on the adsorption capacity of X-LaCl-M. The presence of NOM at concentrations of 5, 50, or 250 mg/L favors F^- adsorption on these SXGs with the exception of X-LaCl-M, which achieves low F^- removal at 50 mg/L OM but increases its adsorption at 250 mg/L OM. In comparison to results in distilled water, F^- adsorption is lower on X-B and X-LaCl-M but unchanged on X-LaCl and X-LaO when tap water is used.

References

Amini, M., Mueller, K., Abbaspour, K.C., Rosenberg, T., Afyuni, M., Møller, K.N., Sarr, M., Johnson, C.A., 2008. Statistical modeling of global geogenic fluoride contamination in groundwaters. Environ. Sci. Technol. 42, 3662–3668.
Andrade-Espinosa, G., Escobar-Barrios, V., Rangel-Mendez, R., 2010. Synthesis and characterization of silica xerogels obtained via fast sol–gel process. Colloid Polym. Sci. 288, 1697–1704.
Andrade Espinosa, G., 2011. Síntesis de xerogeles de sílice como soporte de partículas de hidro (óxidos) de hierro para la absorción de arsénico presente en la solución acuosa.
Cheng, J., Meng, X., Jing, C., Hao, J., 2014. La 3+-modified activated alumina for fluoride removal from water. J. Hazard. Mater. 278, 343–349.
Craig, L., Stillings, L.L., Decker, D.L., 2017. Assessing changes in the physico-chemical properties and fluoride adsorption capacity of activated alumina under varied conditions. Appl. Geochem. 76, 112–123.
Edmunds, W.M., Smedley, P.L., 2013. Fluoride in Natural Waters. Essentials of medical geology. Springer, pp. 311–336.
Fawell, J.K., Bailey, K., 2006. Fluoride in Drinking-water. World Health Organization.
Han, H., Wei, W., Jiang, Z., Lu, J., Zhu, J., Xie, J., 2016. Removal of cationic dyes from aqueous solution by adsorption onto hydrophobic/hydrophilic silica aerogel. Colloid. Surfaces A Physicochem. Eng. Aspects 509, 539–549.
Ivanova, O., Naumkin, A., Vasilyev, L., 1996. An XPS study of compositional changes induced by argon ion bombardment of the LaPO 4 surface. Vacuum 47, 67–71.
Jung, I.-k., Gurav, J.L., Bangi, U.K., Baek, S., Park, H.-H., 2012. Silica xerogel films hybridized with carbon nanotubes by single step sol–gel processing. J. Non Cryst. Solids 358, 550–556.
Landín-Rodríguez, L., 2006. Physicochemical Parameters and Concentrations of Fluoride and Arsenic in Drinkingwater Wells in San Luis Potosí City and Metropolitan Area. Alternative Treatment: Adsorption of Fluoride and Arsenic in the Activated Al2O3/water Solution Interface (Parámetros fisicoquímicos y concentración de flúor y arsénico en el agua de los pozos de ciudad de San Luis Potosí y zona conurbada).
Leyva-Ramos, R., Medellin-Castillo, N.A., Jacobo-Azuara, A., Mendoza-Barron, J., Landin-Rodriguez, L.E., Martinez-Rosales, J.M., Aragon-Piña, A., 2008. Fluoride removal from water solution by adsorption on activated alumina prepared from pseudo-boehmite. J. Environ. Eng. Manage. 18, 301–309.
Lowell, S., Shields, J.E., Thomas, M.A., Thommes, M., 2012. Characterization of Porous Solids and Powders: Surface Area, Pore Size and Density. Springer Science & Business Media.
Martınez, J., Ruiz, F., 2002. Mapeo estructural de sılica xerogel utilizando espectroscopıa infrarroja. Rev. Mexic. Fisica 48, 142–149.
Metcalf, Eddy, Burton, F.L., Stensel, H.D., Tchobanoglous, G., 2003. Wastewater Engineering: Treatment and Reuse. McGraw Hill.
Mohammadi, A., Moghaddas, J., 2015. Synthesis, adsorption and regeneration of nanoporous silica aerogel and silica aerogel-activated carbon composites. Chem. Eng. Res. Des. 94, 475–484.
Mohapatra, M., Anand, S., Mishra, B.K., Giles, D.E., Singh, P., 2009. Review of fluoride removal from drinking water. J. Environ. Manage. 91, 67–77.
Perdigoto, M.L.N., Martins, R.C., Rocha, N., Quina, M.J., Gando-Ferreira, L., Patrício, R., Durães, L., 2012. J. Colloid Interface Sci. 380, 134–140.
Richards, L.A., Vuachere, M., Schafer, A.I., 2010. Desalination 261, 331–337.
Sanchez-Polo, M., Rivera-Utrilla, J., Salhi, E., Von Gunten, U., 2007a. Ag-doped carbon aerogels for removing halide ions in water treatment. Water Res. 41, 1031–1037.
Sánchez-Polo, M., Rivera-Utrilla, J., von Gunten, U., 2007b. Bromide and iodide removal from waters under dynamic conditions by Ag-doped aerogels. J. Colloid Interface Sci. 306, 183–186.
Tang, Y., Guan, X., Wang, J., Gao, N., McPhail, M.R., Chusuei, C.C., 2009. Fluoride adsorption onto granular ferric hydroxide: effects of ionic strength, pH, surface loading, and major co-existing anions. J. Hazard. Mater. 171, 774–779.
Teutli-Sequeira, A., Martínez-Miranda, V., Solache-Ríos, M., Linares-Hernández, I., 2013. Aluminum and lanthanum effects in natural materials on the adsorption of fluoride ions. J. Fluorine Chem. 148, 6–13.
Yakun, H., Wenming, D., Huang, X., Jingnian, X., Menghua, Z., 2011. Fluoride removal by lanthanum alginate bead: adsorbent characterization and adsorption mechanism. Chin. J. Chem. Eng. 19, 365–370.